

1
2 UNIVERSITY OF NEBRASKA - LINCOLN
3 *Physics & Astronomy*

4 COMPREHENSIVE EXAMINATION

5
6 **The Observation of Gravity waves at LIGO**

7
8 *Author:*

Caleb FANGMEIER

Supervisory Committee:

Dr. Gregory SNOW (Chair)

Dr. Christian BINEK

Dr. Daniel CLAES

Dr. Sebastian ELBAUM

Dr. Ilya KRAVCHENKO

9 **Abstract**

10 *On September 14, 2015 09:50:45 UTC, the first direct observation of a gravitational wave was made by the Advanced*
11 *LIGO experiment. The event, deemed GW150914[1], was determined to be caused by the inspiral and subsequent merger*
12 *of two stellar-mass black holes. Subsequently, on December 26, 2015 03:38:53 UTC another black hole merger event was*
13 *observed[2]. These two observations confirm the predictions of general relativity in the highly non-linear strong field*
14 *regime as well as cosmological predictions of the existence of binary black hole systems. Here I discuss the theoretical*
15 *mechanisms enabling the observation of gravitational waves, the design of the Advanced LIGO detector, the extraction of*
16 *events from data, and the implications to various cosmological models.*

17
May 24, 2017

I. INTRODUCTION

IN 1916, Einstein predicted the existence of gravity waves as a consequence of his theory of general relativity. However, despite a century of experimental effort, direct observation eluded scientists until September 2015 when the Advanced Laser Interferometer Gravitational-Wave Observatory (LIGO) observed a gravity wave resulting from a binary black hole merger.

The structure of this paper is as follows: In Section II I will go through the history of gravitational waves beginning with their first theoretical predictions and continuing through early efforts at direct detection by Weber and others. Section III is a rather thorough description of the Advanced LIGO detector itself. Section IV describes the data analysis strategies employed to find evidence of gravity waves in the data coming from the detector. Section V describes the two published gravity wave observations made in the first observing run of Advanced LIGO. Section VI Briefly describes some of the implications of the observed events on cosmology. And finally Section VII gives some closing remarks.

II. THE HISTORY OF GRAVITY WAVES

In this section, I give an overview of some of the history of gravity waves from their tumultuous theoretical origins to early efforts at detection.

i. The Existential Question

In 1905 Henri Poincare published a paper entitled “Sur la dynamique d’ l’electron”[3]. In the paper, Poincare described his theory of relativity which based the existence of gravity waves on analogy with the electromagnetic waves produced by accelerating charges. However, it would take until 1916 for Einstein to publish his Theory of General Relativity[4]. This theory, which was in many ways an extension of his Theory of Special Relativity, viewed gravity not as a force, a la Newton, but instead as a curvature in space-time brought about by the presence of mass and energy. Expressed mathematically, Einstein’s field equations can be written in tensor form as

$$R_{\mu\nu} - \frac{1}{2}Rg_{\mu\nu} + \Lambda g_{\mu\nu} = \frac{8\pi G}{c^4}T_{\mu\nu}$$

where $R_{\mu\nu}$ is the Ricci curvature tensor, R is the scalar curvature, $g_{\mu\nu}$ is the metric tensor, Λ is the cosmological constant, G is Newton’s gravitational constant, and $T_{\mu\nu}$ is the stress-energy tensor.

Roughly speaking, the right-hand side of the equation is determined by a distribution of mass and energy and the left-hand side represents the resulting space-time curvature. Unfortunately, although the equation appears relatively simple, both the Ricci tensor and the scalar curvature depend on the metric tensor in a complicated nonlinear manner. As a result, in only a small number of cases with readily exploitable symmetries have the field equations been solved analytically. In fact, it has taken great efforts in the field of Numerical Relativity to be able to obtain the necessary theoretical results for LIGO to know what the signature of various astronomic calamities (e.g. binary black-hole mergers) would look like.

But back 1916, Einstein was still grappling with his nascent theory and its implications. For example, because there is no such thing as negative mass in General Relativity (in contrast to electro-magnetism where charge comes with positive *and* negative signs), one cannot construct a gravitational dipole or resulting dipole radiation. By 1936, Einstein, together with his student Nathan Rosen, had arrived at the conclusion that gravity waves could not exist in the theory. Indeed, they submitted a paper to the *Physical Review* stating as much. The editor forwarded the paper to the referee, a Howard Percy Robertson, who pointed out several flaws in the paper. Einstein, apparently unfamiliar with the peer review process, responded to the criticism.

July 27, 1936

Dear Sir,

“We (Mr. Rosen and I) had sent you our manuscript for publication and had not authorized you to show it to specialists before it is printed. I see no reason to address the-in any case erroneous-comments of your anonymous expert. On the basis of this incident I prefer to publish the paper elsewhere.”

Respectfully

56 Einstein

57 P.S. Mr. Rosen, who has left for the Soviet Union, has authorized me to represent him in the matter.

58 With the departure of Rosen, another young physicist named Leopold Infeld became the new assistant
59 to Einstein. Infeld befriended Robertson (the referee who criticized the original paper) and together they
60 confirmed the error in the original Einstein-Rosen submission. Infeld proceeded to point out the error to
61 Einstein who was then obligated to submit a letter to the editor of the *Journal of the Franklin Society* where he
62 had eventually submitted the paper after its rejection by *Physical Review*. The revised paper contained the
63 following conclusion.

64 "Rigorous solution for Gravitational cylindrical waves is provided. For convenience of the reader the theory of
65 gravitational waves and their production, known in principle, is presented in the first part of this article. After
66 finding relationships that cast doubt on the existence of gravitational fields rigorous wavelike solutions, we
67 have thoroughly investigated the case of cylindrical gravitational waves. As a result, there are strict solutions
68 and the problem is reduced to conventional cylindrical waves in Euclidean space."

69 In the end Einstein came to understand that gravitational waves were a real part of General Relativity.
70 However, it remained to be seen how such waves could be seen in experiment.

71 ii. Physical Interpretations

72 Unfortunately for the experimentalist, the coordinate systems commonly employed for calculations in the
73 realm of General Relativity were chosen for reasons of mathematical simplicity, not for easily extracting
74 observables or making comparisons with experiment. In 1956, Felix A. E. Pirani addressed this problem in
75 his paper "On the physical significance of the Riemann tensor"[5]. In his paper, Pirani deduced the effects of
76 space-time curvature to an observer in an inertial frame. Crucially, Pirani showed that particles are oscillated
77 by the passing of a gravity wave.

78 It is worth taking a slight pause in the story here to describe in greater detail the physical nature of gravity
79 waves. First of all, these waves travel at the speed of light, which could be seen as either a direct consequence
80 of General Relativity, or a result of a massless graviton. The stretching and squeezing of space is always
81 and only transverse to the direction of propagation and is invariant under a 180° rotation around the axis of
82 propagation. The waves come in two polarizations, the $+$ polarization, which affects free particles as depicted
83 in Fig. 1, and the \times polarization which is rotated 45° with respect to the $+$ polarization. These waves can
84 be red shifted and gravitationally lensed, just like electro-magnetic waves. However, unlike electro-magnetic
85 waves, they are only negligibly dispersed by interactions with matter[6].

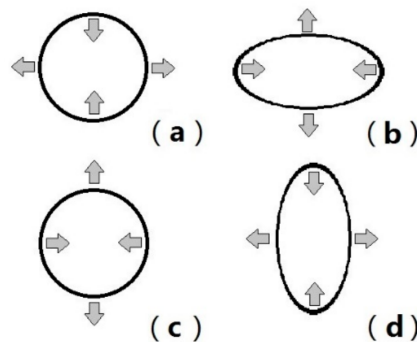


Figure 1: The effect of a $+$ polarized gravitational wave propagating into the page on a ring of free particles. Initially, the particles form a circle (a), but as the wave passes into the page, space is stretched horizontally, and squeezed vertically (b). A half-period later, however the situation is reversed and space is squeezed horizontally and stretched vertically (d).

86 In the year following Pirani's paper, the seminal Chapel Hill conference was held on the campus of the
87 University of North Carolina, and among the many notable attendees were Richard Feynman, Julian Schwinger,
88 and John Wheeler. The conference has organized by the Institute of Field Physics (IOFP), under the patronage

89 of eccentric millionaire Roger W. Babson. Of the many topics covered at the six day conference, one of the
90 most hotly debated was the question of whether gravity waves were able to carry energy. To address this
91 question, Feynman, in characteristic style, anonymously proposed a simple thought experiment known as the
92 “sticky bead” experiment. It goes as follows.

93 Consider a rod threaded through two rings as depicted in Fig. 2. The rings are allowed to slide along the
94 rod, but there is some small friction between the rings and the rod. As a gravity wave traverses the experiment,
95 space will get periodically stretched and compressed along the axis of the rod, meaning the proper-distance
96 between the rings oscillates. On the other hand, the atomic restoring forces between the atoms in the rod
97 will keep its length fixed. Consequently, the rings will rub against the rod, heating it. This implies that the
98 gravitational wave is doing work on the system, and must therefore carry energy.

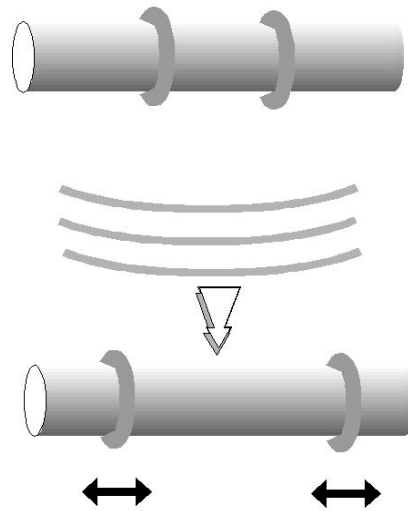


Figure 2: Sketch of the “sticky bead” experiment.[7].

99 Also at the Chapel Hill conference was an engineer from the University of Maryland named Joseph Weber.
100 He was fascinated by the phenomena of gravitational waves. So much so, that he went on to design the first
101 experiment to directly detect them.

102 iii. Early Experimental Efforts

103 In the years following the Chapel Hill conference Weber designed a ground based “antenna” which could
104 detect the presence of gravity waves. He detailed his ideas in his 1960 paper “Detection and Generation of
105 Gravity Waves”[8], and by 1966 had built a detector and published evidence of its performance[9].

106 Weber’s experimental setup consisted of a large aluminum cylinder, 66cm in diameter and 153cm in
107 length[10]. The cylinder was suspended by steel wires from a vibration isolating support. Piezoelectric sensors
108 were mounted around the diameter of the cylinder to detect vibrations, such as those induced by passing
109 gravitational waves.

110 Weber actually built two of these detectors: one at the University of Maryland, and another nearly 1000 km
111 away at Argonne National Laboratory outside Chicago, with the idea being to use them to cross-check each
112 other and eliminate false positives from local noise sources.

113 Amazingly, when Weber turned on his detectors, they picked up about one coincidence a day. He claimed
114 this as evidence for the discovery of gravity waves. He went further to claim that many of the signals originated
115 near the center of our galaxy and estimated from his measurements that our galaxy is radiating ≈ 1000 solar
116 masses per year of energy in the form of gravity waves. This ran afoul of estimates from cosmologists who
117 calculated an upper limit of 200 solar masses per year. Any larger, and the necessary mass to hold the galaxy
118 together would have radiated away long ago.

119 A hallmark of all good science is repeatability. As such, efforts were undertaken by others to build similar
120 resonating bar experiments to attempt to reproduce Weber’s results. By the middle of the 1970s several
121 additional experiments were running that incorporated improvements over Weber’s original design such as

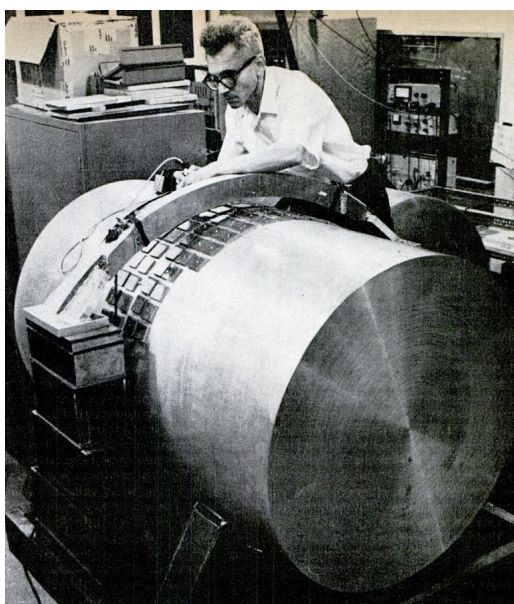


Figure 3: Weber working on his detector

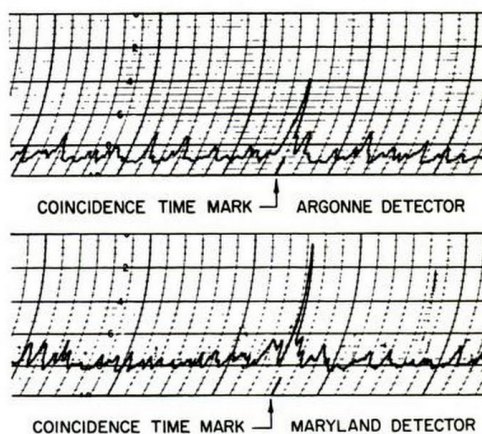


Figure 4: An example of a detector coincidence seen by Weber published in the May 1972 issue of Popular Science

122 cooling the cylinders to reduce thermal noise. Sadly, none of these improved detectors were able to reproduce
 123 Weber's results. This inability to confirm Weber's results, combined with the unresolved disagreement with
 124 astronomic observations convinced most members of the community that Weber's original observations were
 125 spurious.

126 With efforts at direct observation of gravity waves stymied for the moment, indirect observations would
 127 have to do. This came in the form of the observation of orbital decay in a binary pulsar system by Taylor
 128 and Hulse[11]. They used a 305 m diameter radio telescope to observe the electro-magnetic emissions of the
 129 pulsar over time and deduce changes in the relative distance between the earth and the pulsar over a period of
 130 several years. They then fit these measurements to a model to find the orbital period of the binary pulsar.

131 Their results (including measurements made after their original publication in 1979) are shown in Fig. 5.
 132 As the pulsars orbit each other, they emit quadrupole gravitational radiation which removes kinetic energy
 133 from the system. As a result the orbital period decreases with time. This is precisely what was observed
 134 by Taylor et al. and their observations matched the predictions of General Relativity remarkably well, and
 135 excluded other theories of gravitation that predicted gravitational dipole radiation.

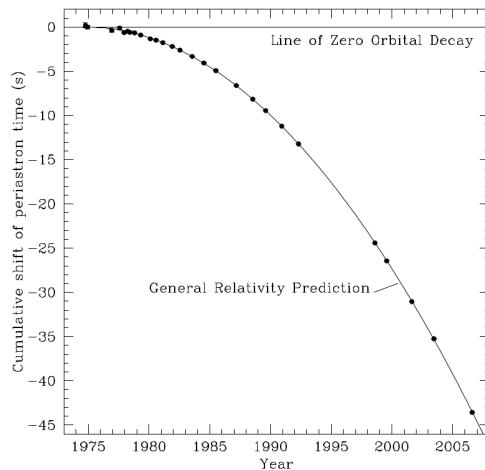


Figure 5: The decay of the orbital period of PSR1913 due to the emission of gravity waves

136 iv. First Generation Interferometers

137 Given the lack of reproducible results from the Weber bar experiments, experimentalists began investigating
 138 completely different types of detectors for direct detection, the most promising of which was the laser
 139 interferometer. The earliest use of an interferometer to detect gravity waves was made by a former student of
 140 Weber named Robert Forward. Forward's detector (Fig. 6) consisted of 8.5 m arms and through 150 hours of
 141 observation found no coincidences with the Weber bar detectors simultaneously in operation[12].

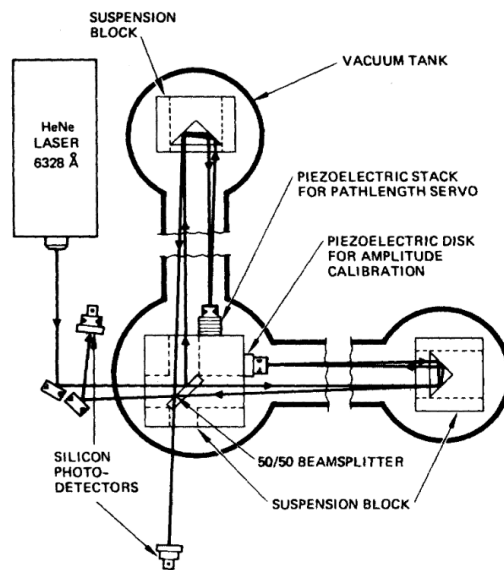


Figure 6: A schematic of Robert Forward's early interferometer. Note the multiple paths the laser takes through each leg of the detector and the two photo-detectors, used to mitigate electronic noise.

142 The idea was not dead, however, and by the mid 1990s there were several large collaborations working on
 143 constructing long baseline interferometers. These included the GEO600 experiment in Germany, Virgo in Italy,
 144 and, of most relevance here, LIGO in the United States.

145 The inception of what would eventually become LIGO happened in the summer of 1975 when Rainer
 146 Weiss, an experimentalist at MIT, and Kip Thorne, a theorist from Caltech, met at a conference hosted by
 147 NASA to explore the applications of space-based research to cosmology and relativity. As Thorne did not have
 148 a hotel room, he shared one with Weiss who recalls that night,

149 “We made a huge map on a piece of paper of all the different areas in gravity. Where was there a
150 future? Or what was the future, or the thing to do?”[13]

151 Inspired by his conversation with Weiss, Thorne decided that the thing to do at Caltech was to develop
152 interferometers to detect gravity waves, and to accomplish this, he brought in an experienced experimentalist,
153 Ronald Drever, to construct the detectors. For several years Weiss and Drever competed from opposite coasts
154 to create better and better interferometers. Eventually both groups came to the conclusion that a discovery
155 strength interferometer would have to be constructed at such a scale that attracting funding for separate
156 experiments would be impossible. Therefore, with some prodding by the NSF, the Caltech and MIT groups
157 joined forces and formed the “Laser Interferometer Gravitational-Wave Observatory” (LIGO).

158 Unfortunately, the triumvirate of Thorne, Weiss, and Drever proved unable to effectively manage the project
159 so in 1986 the NSF instead appointed Rochus E. Vogt as the single project manager[14]. Despite this reshuffling
160 of leadership, progress was slow and by 1994 Drever had left the project and Vogt was replaced with Barry
161 Clark Barish¹, an high-energy experimentalist who had experience working in large collaborations. Under
162 Barish’s leadership, the original plan for LIGO was reworked into a two-stage deployment. The first stage,
163 named Initial LIGO, or iLIGO, would include the construction of two laboratories, one in Hanford, Washington,
164 and the other in Livingston, Louisiana. They would be built with current generation interferometers that
165 would serve as a proof-of-concept and development platform for the second stage, known as Advanced LIGO.
166 Advanced LIGO would use the same facilities as iLIGO, but replace the interferometers with next-generation
167 designs.

168 Barish also suggested splitting the experiment into two separate entities. The first would be responsible for
169 the administration and operation of the laboratory facilities, and the other, the “Ligo Scientific Collaboration”,
170 would be in charge of scientific and technological research, as well as forging alliances with other collaborations,
171 most notably GEO600 and Virgo.

172 Initial LIGO begin construction in 1995 and finished in 1997, however it still took until 2002 to begin taking
173 scientific data, whereupon it operated in months long runs across eight years before ceasing operation in 2010,
174 having not yet observed gravity waves. This was not unexpected as the intention had always been to use Initial
175 LIGO as a research and development platform to design Advanced LIGO, and the odds of actually making an
176 observation with Initial LIGO were small.

177 III. THE ADVANCED LIGO DETECTOR

178 After The shutdown of Initial LIGO, efforts promptly began to install the upgraded systems of Advanced
179 LIGO, and by February 2015[15], the experiments began taking “engineering mode” data to commission the
180 new systems. And finally, in September of that same year began taking scientific data.

181 i. Principle of Operation

182 LIGO is at its heart a Michelson style interferometer. This type of interferometer is displayed schematically in
183 Fig. 7. The interferometer works by first producing a coherent light source, typically a laser, and then splitting
184 the source into two beams that take different paths. The beams are then recombined and made to interfere
185 with each other. The resulting interference pattern can then be used to infer the difference in the path lengths
186 taken by the two lasers, or at least the distance modulo the wavelength of the laser.

187 If the two path lengths are exactly the same, the lasers will combine constructively and stimulate the
188 sensitive element (e.g. a photo-diode) in the detector. However, as the path lengths diverge, the two beams
189 will begin to interfere destructively and the resulting signal seen by the detector will decrease in amplitude
190 until it disappears entirely when the path length differ by a half-wavelength.

191 In the case of LIGO, the nominal operating point is destructive interference at the detector, at the so-called
192 “dark fringe”. Accordingly, the detector end of the interferometer is referred to as the “dark port”. As a gravity
193 wave passes through the detector, it causes one leg of the detector to lengthen and the other to contract. This
194 differential change in length appears as a departure from perfect destructive interference, and the larger the
195 amplitude of the wave, the larger the signal seen by the photo-detector.

¹Born in Omaha, NE

196 It may be tempting to think that just as the space between the test masses (the splitter and the mirrors)
 197 gets stretched and squeezed with the passing of the gravity wave, so does the wavelength of the laser pulse
 198 leading to no observable change in the interference pattern. It turns out that this is not the case. Although the
 199 laser's wavelength *does* get stretched and squeezed by the passing gravity wave, the effect is approximately
 200 ten-thousand times smaller than the effect on the test masses, well below the noise floor of LIGO. This is due
 201 to the fact that the spatial extent of LIGO (≈ 4 km) is much smaller than the wavelength of the gravity waves
 202 being searched for (≈ 3000 km).

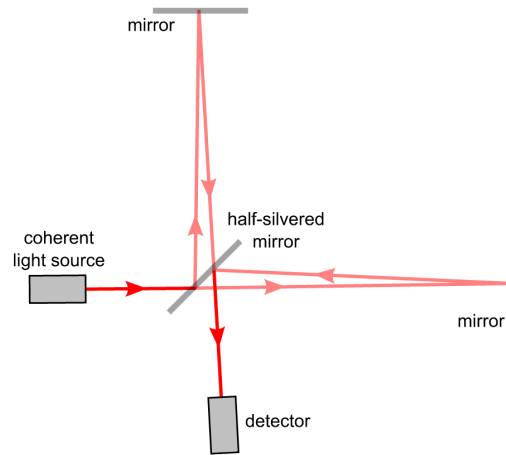


Figure 7: Schematic representation of a Michelson interferometer. Image credit: Wikipedia

203 Unfortunately a simple Michelson interferometer would not be sensitive enough to detect the tiny deforma-
 204 tions from gravity waves. The limitation comes from the Michelson interferometer requiring a differential
 205 deformation on the order of λ to shift from fully constructive to fully destructive interference. A typical strain,
 206 defined as $h \equiv \frac{1}{2} \frac{\Delta l}{l}$, for the types of waves LIGO is searching for is $h \approx 10^{-21}$ which gives a corresponding
 207 deformation of $4 \text{ km} * 10^{-21} = 4 \times 10^{-9} \text{ nm}$ which is about twelve orders of magnitude smaller than λ . With
 208 such a large disparity, the resulting phase change would be too tiny to create a measurable deviation from the
 209 dark-fringe. Clearly, a way to get much larger phase shifts for an amount of deformation is needed.

210 Enter the Fabry-Pèrot Interferometer, or more specifically as one end is almost a perfect mirror, the
 211 Gires-Tournois Interferometer[16]. In addition to the optical elements of the Michelson interferometer, this
 212 device adds an additional optical element in each leg between the beam splitter and the outer mirror. The
 213 cavity formed by the new element and the outer mirror is tuned to be resonant with the incident laser. The
 214 Advanced LIGO setup is shown in Fig. 8.

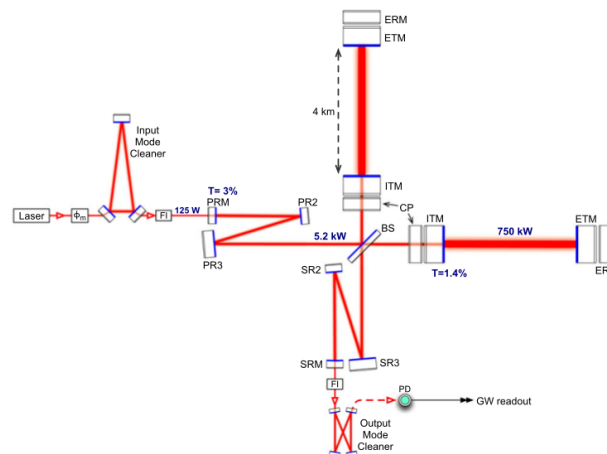


Figure 8: The Advanced LIGO optical configuration.[17].

The Fabry-Pèrot resonance chamber in each leg is formed at one end by the end test mass (ETM) and at the other by the input test mass (ITM). The surface of the ETM is a nearly perfect mirror (transmission of 5 ppm), and the ITM has a reflection coefficient close to unity ($R = 98.6\%$). This configuration provides an output signal whose phase is highly dependent on changes to the quantity

$$\delta \equiv \frac{4\pi}{\lambda} nL \cos \theta_L.$$

In the case of LIGO, n , the index of refraction in the chamber, is 1 since the laser is propagating through vacuum, λ , the wavelength of the laser is 1064 nm, and θ_L , the angle of refraction is zero as the laser is normally incident. Assuming these variables are well controlled, δ will depend only on L , the length of the resonant cavity.

As a function of δ , the (complex) reflectivity is

$$r = -\frac{r_1 - e^{-i\delta}}{1 - r_1 e^{-i\delta}}$$

where r_1 is the internal reflectivity of the ITM. If we assume that there are no losses in the resonator, r_1 is real and $|r_1| = 1$. However, r will still have a phase shift given by

$$\tan\left(\frac{\Phi}{2}\right) = -\frac{1 + \sqrt{R}}{1 - \sqrt{R}} \tan\left(\frac{\delta}{2}\right).$$

Where $R = |r_1|^2$. In reality, there are losses in the dielectric coatings of both the ETM and the ITM, but great care has been taken to make these losses small².

If we now rewrite L in terms of the gravitational strain, h

$$L = L_0 + \Delta L = L_0(1 + h),$$

we get

$$\Phi = -2 \tan^{-1}\left(\frac{1 + \sqrt{R}}{1 - \sqrt{R}} \tan \frac{\delta}{2}\right); \delta = 4\pi \frac{4 \text{ km}}{1064 \text{ nm}} (1 + h)$$

To illustrate how this improves the sensitivity of the detector for small values of h , Fig. 9 shows the phase shift as a function of strain for different internal reflectivities. Note that the $R = 0$ case corresponds to the normal Michelson interferometer where the ITM is transparent to the returning laser. As R tends towards unity, a more and more non-linear response appears due to increasing interference of the beam with itself after multiple traversals of the interferometer leg. This means that much better sensitivity to small h can be achieved by pushing R towards 1. Of consequence to the following discussion is the quantity known as *finesse*. It can be defined as

$$\mathcal{F}_c \equiv \frac{2\pi}{-\ln(R_1 R_2)},$$

where R_1 and R_2 are the intensity reflectivities of the mirrors on either end of the Fabry-Pèrot cavity. Qualitatively, as the product of the reflectivities approaches unity, the finesse becomes large. In practice the finesse is adjusted to balance the power stored in the cavity, and the sharpness of the transmission/reflection curves as a function of frequency.

ii. The Laser Source and Input Optics

LIGO employs a multi-stage neodymium-doped yttrium aluminum garnet (Nd:YAG) laser that can supply up to 180 W of power to the interferometer. The laser source together with initial stabilizing and cleaning optics are referred to as the pre-stabilized laser (Fig. 11).

The laser cavity produces radiation with a nominal wavelength of 1064 nm, and frequency power distribution as shown in Fig. 10 a.

²The drastically increased circulation power in Advanced LIGO, however, causes appreciable heating of the optics, leading to thermal lensing. Compensating heaters are added to the lenses to mitigate this effect. The fractional losses are still small enough, however, to make the following calculations valid.

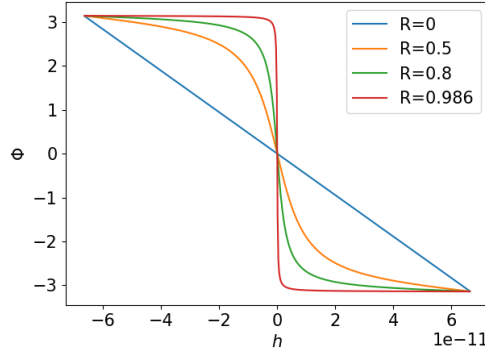


Figure 9: Relations between the phase-shift, Φ , and h for various values of internal reflectivity R .

231 To understand this figure, first note that the radiation produced by a laser cavity can be decomposed into
 232 transverse modes (see Fig. 10 b). The presence of higher-order transverse modes in the beam is a problem
 233 because, due to the Gouy phase shift, the frequencies of these modes are higher than the frequency of the
 234 TEM_{00} mode. Since the interferometer is extremely sensitive to changes in laser frequency, it is therefore
 235 crucial to remove these other modes as much as possible. To that end, the beam is passed through the
 236 pre-mode-cleaner (PMC). This is a bow-tie cavity that strips higher-order modes from the beam. For example,
 237 it reduces the amplitudes of the TEM_{01}/TEM_{10} modes by a factor of 63. It also serves to provide low-pass
 238 filtering of RF intensity fluctuations.

239 After passing through the PMC, the beam goes through a RF modulator which adds low-amplitude phase
 240 modulation at 9 MHz, 45 MHz, and 24 MHz. The 9 and 45 MHz modulations are used for global sensing of the
 241 interferometer, while the 24 MHz modulation is used for input-mode-cleaner (IMC) sensing. These side bands
 242 are used by the Pound-Drever-Hall[18] stabilization method. For a thorough description of the technique
 243 see [19]. Pound-Drever-Hall can be used for both laser frequency stabilization and Fabry-Pèrot cavity length
 244 stabilization. In fact, LIGO uses variations of the technique for both.

To illustrate the Pound-Drever-Hall method for laser frequency stabilization, consider a laser shining into
 a Fabry-Pèrot cavity with identical mirrors on either end. The laser is equipped with an actuator that can
 deform the lasing cavity to slightly alter the laser's frequency allowing for active correction of deviations from
 the ideal frequency. The transmission function of the cavity is given by

$$T_e = \frac{T^2}{1 + R^2 - 2R \cos\left(\frac{2L}{c}(\omega_0 + \Delta\omega)\right)},$$

245 where R and T are the reflection and transmission coefficients of the cavity mirrors, L is the length of the
 246 cavity, ω_0 is the ideal, resonant, frequency in the cavity, and $\Delta\omega$ is a deviation from that ideal.

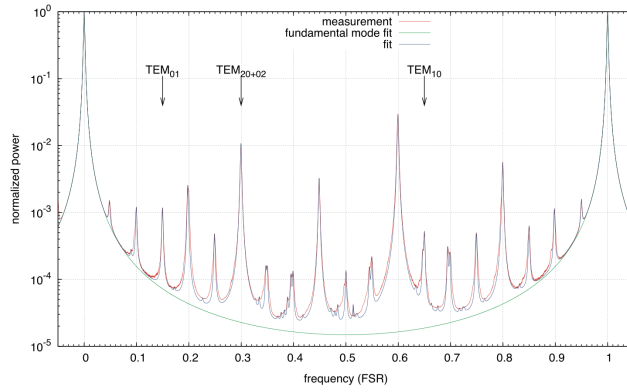
Of more interest for Pound-Drever-Hall is the reflectivity (Fig. 12) given simply by

$$R_e = 1 - T_e.$$

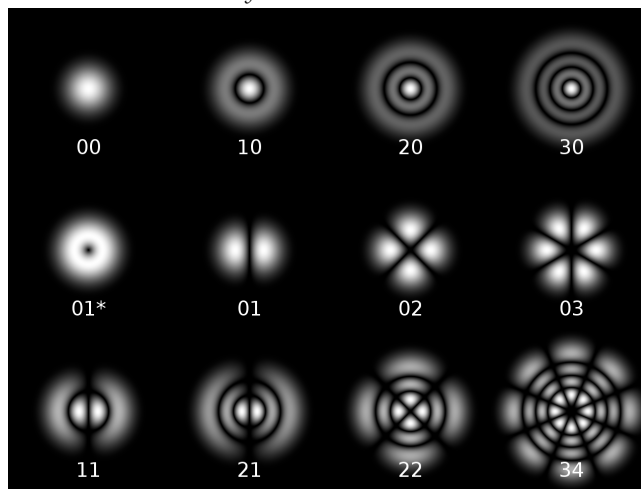
247 Now, a detector can be placed on the upstream side of the cavity to sense reflected light. If the detector sees
 248 anything, one can infer that the detector is off resonance, and the laser frequency has deviated from its ideal
 249 value³. Unfortunately, the error signal is symmetric about the resonance so the actuator in the lasing cavity
 250 does not know which way to adjust the laser to correct the error. Pound-Drever-Hall solves this by introducing
 251 a small phase modulation to the laser to operate the cavity slightly off resonance.

252 The modulated error signal then sinusoidally traces the reflection curve in the area highlighted by the
 253 inset of Fig. 12. If the frequency is too high, the error will trace up and down the curve on the right side of
 254 the minimum so the error signal will be in phase with the modulating signal implying that the product of
 255 the error and modulation signal will be positive. On the other hand, if the frequency is too low, the signals

³Note that this is in contrast with the LIGO arm cavities where the intensity of the reflected light is independent of laser frequency or arm length. In this case, the equation for T_e does not apply since the two ends have differing reflectivities. The applicable error signal in this case is the light shining into the dark port.



(10 a) Mode scan of the laser used at the Livingston Detector demonstrating that nearly 95% of the laser's energy is in the TEM₀₀ mode. The horizontal scale is in units of free spectral range (FSR) which is defined as $\frac{c}{2L}$ where L is the length of the resonant cavity.



(10 b) Intensity distributions of transverse laser modes for a cylindrically symmetric beam. Image Credit: Wikipedia

256 will be half a period out of phase so the product will be negative. Therefore, by simply observing the sign of
 257 the product of the error signal and the modulating signal, the control system knows whether to adjust the
 258 frequency up or down.

259 In a similar way, if the laser frequency is assumed stable, but the length of the cavity is varying, the same
 260 scheme can be applied with the only substantive difference being the actuator now applies a force to one or
 261 both of the cavity mirrors instead of the lasing cavity. This is the method used to keep all of the LIGO optical
 262 resonant cavities on their working point.

263 After modulation, the beam passes through the final stage of the pre-stabilized laser system, the input-mode-
 264 cleaner. The input-mode-cleaner is used to further fix the laser's mode content, as well as stabilize the beam's
 265 position as it shines onto the power recycling mirror (PRM). Using the 24 MHz modulation and the Pound-
 266 Drever-Hall locking technique, it is able to help stabilize the frequency of the laser to $< 1 \times 10^{-3} \text{ Hz}/\sqrt{\text{Hz}}$ at
 267 100 Hz.

268 Finally, before being passed to the core optics of the interferometer, the beam passes through a Faraday
 269 Isolator which prevents light that is returning from the core optics from creating parasitic effects in the input
 270 chain.

271 iii. Core Optics

272 The output of the PSL is routed into the core interferometer optics. These consist of one ETM and one ITM for
 273 each leg. Adjacent to each ITM, there is also a compensation plate (CP) which used used as a reaction mass

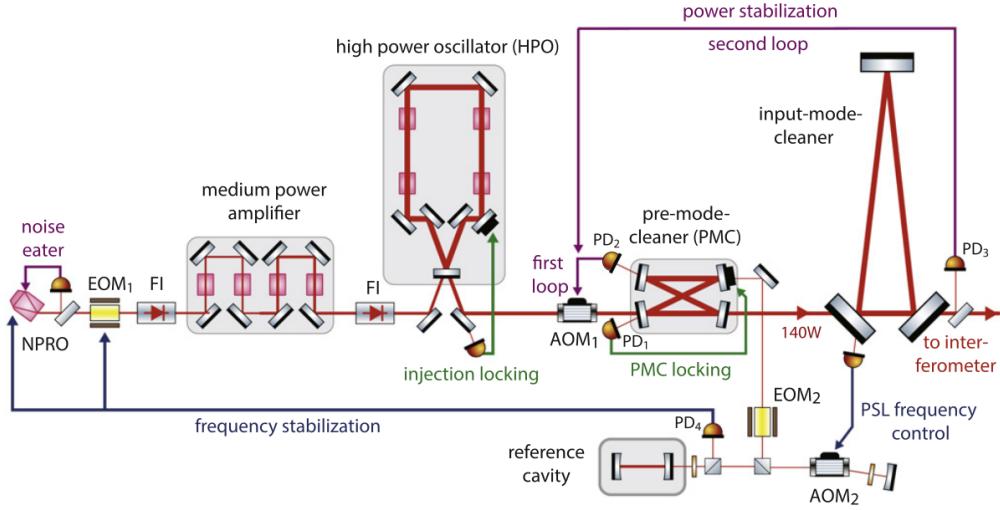


Figure 11: Schematic of the pre-stabilized laser system. AOM: acousto-optic modulator, EOM: electro-optic modulator, FI: Faraday isolator, PD: photodetector

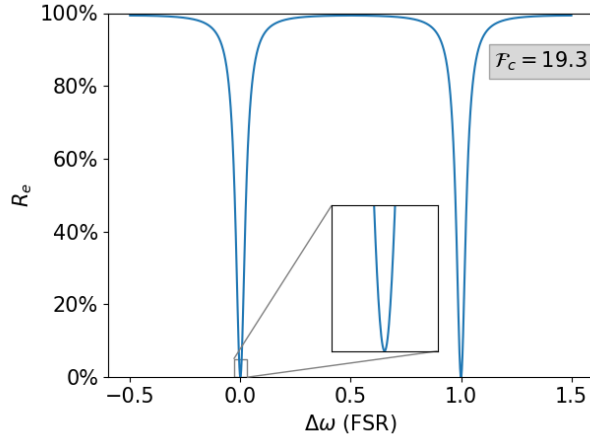


Figure 12: The reflection coefficient of a Fabry-Pèrot cavity as a function of $\Delta\omega$, i.e. deviations in laser frequency.

274 for actuating the ITM. Similarly, there is a end reaction mass for actuating the ETM.
 275 The actuation of these optics is accomplished by applying a circular thin gold plating on the reaction
 276 masses that can be made to hold an electro-static charge by application of a voltage. This charge will push or
 277 pull on the dielectric test mass. The plating is divided into quadrants to also allow for aiming the test mass.
 278 Initial LIGO actually affixed magnets to the test masses and applied forces to the magnets via magnetic fields
 279 induced by coils mounted on the reaction masses. The electro-static method is preferred because mounting
 280 magnets on the test masses modifies their natural vibration modes, leading to additional thermal noise.
 281 To round out the core optics, there is a 50/50 beamsplitter, four curved mirrors for signal (SR2, SR3) and
 282 power (PR2, PR3) recycling as well as the partially transmitting power recycling mirror (PRM) and signal
 283 recycling mirror (SRM). Parameters for all these core optics, including dimensions, mass, transmission rates,
 284 radii-of-curvature, and beam size on the optic, are shown in Table 1.
 285 One of the key improvements from Initial LIGO to Advanced LIGO was the addition of the signal recycling
 286 system. This can be seen in Fig. 8 as the elements SR2, SR3, and SRM. This serves to reshape the response of
 287 the interferometer to be more sensitive to signals in the low-audio frequency band that would be come from
 288 binary neutron star or black hole coalescences[20]. The parameters of the signal recycling subsystem can be
 289 adjusted to enhance other frequency bands as well.

Optic	Diameter \times thickness (cm)	Mass (kg)	Transmission	ROC (m)	Beam size (cm)
ITM	34 \times 20	40	1.4% (0.5-2%)	1934	5.3
ETM	34 \times 20	40	5 ppm (1-4%)	2245	6.2
CP	34 \times 10	20	AR < 50 ppm	flat	5.3
ERM	34 \times 13	26	AR < 1000 ppm	flat	6.2
BS	37 \times 6	14	50%	flat	5.3
PR3	26.5 \times 10	12	<15 ppm	36.0	5.4
SR3	26.5 \times 10	12	<15 ppm	36.0	5.4
PR2	15 \times 7.5	2.9	225 ppm (>90%)	-4.56	0.62
SR2	15 \times 7.5	2.9	<15 ppm	-6.43	0.82
PRM	15 \times 7.5	2.9	3.0%	-11.0	0.22
SRM	15 \times 7.5	2.9	20%	-5.69	0.21

Table 1: Parameters for the core optics. All transmission values are at 1064 nm, except for those in parentheses which are for 532 nm. AR: anti-reflection

iv. Environmental Isolation

A great disadvantage of terrestrial experiments is that they are subject to the whims of nature, be it turbulent weather, the rumblings of the earth, or, in the case of the Livingston experiment, particularly heavy-footed alligators⁴. In fact, the ground motion at the sites of the two LIGO detectors is measured to be $\sim 10^{-6}$ m/ $\sqrt{\text{Hz}}$ while the perturbations from gravity waves are $\sim 10^{-18}$ m/ $\sqrt{\text{Hz}}$. This twelve order of magnitude difference emphasizes the importance, and the difficulty, of isolating the experiment from environmental vibrations.

The environmental isolation system is divided into two parts. The subsystem closest to the ground is referred to as the seismic isolation system, and the subsystem between that and the test masses is the suspension system.

The seismic isolation system, shown in some detail in Fig. 13. It consists of first the Hydraulic External Pre-Isolator (HEPI) system that uses a blend of geophones and inductive position sensors together with hydraulic actuators to actively damp low frequency (0.1 Hz-10 Hz) vibrations. This supports the Internal Seismic Isolation (ISI) system. The ISI sits inside vacuum and consists of three stages (labeled in the figure as Stage 0, Stage 1, and Stage 2) are sequentially suspended and sprung from each other. The stages are instrumented with capacitive position sensors and controlled with electromagnetic force actuators. The stage 2 structure includes an optics table from which the optical elements are suspended.

All of the in-vacuum core optics are mounted on elaborate multi-stage suspension systems of various designs based on noise requirements. Table 2 lists these noise requirements along with number of spring-based vertical isolation stages, pendulum stages, and suspension wire types. An example of all of these things put together, in this case for the ITM, is shown in Fig. 14.

A pendulum suspension is a wonderful choice for passive filtering of environmental vibrations due to the property that above its resonance frequency, ω_0 , it suppresses noise by a factor of ω_0^2/ω^2 . And this property can be chained by hanging pendula from other pendula. For the test masses, there are four pendula stages, yielding filtering $\propto \omega^{-8}$ for ω greater than all the resonance frequencies of the system. Unfortunately, this only serves to damp horizontal motion, and, although horizontal noise in the test masses causes the most direct damage to signal quality, vertical and angular misalignment also contribute. To provide for isolation from vertical noise,

IV. SIGNAL EXTRACTION

The raw signal coming from the photo-diodes at the dark port are unsuitable for direct analysis because it contains a convolution of the gravity wave strain with the detector's response. The gravity wave signal, h is proportional to the differential length change, $\Delta L_{\text{free}} = L_x - L_y = hL$, where $L \equiv (L_x + L_y)/2$ is the average arm length. By rearranging the equation, we get $h = \Delta L_{\text{free}}/L$. Now, the control system of LIGO does not actually allow for the lengths to change freely. Instead, it actuates the test masses to compensate for the strain

⁴not measurable

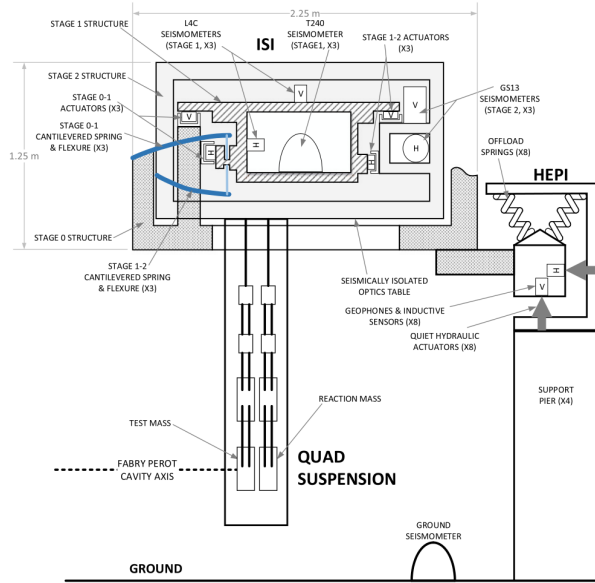


Figure 13

Optical component	Vertical iso. stages	Pendulum stages	Final stage fibre type	Longitudinal noise requirement @ 10 Hz ($m/\sqrt{\text{Hz}}$)
Test masses (ITM, ETM)	3	4	Fused silica	1×10^{-19}
Beamsplitter (BS)	2	3	Steel wire	6×10^{-18}
Recycling cavity optics	2	3	Steel wire	1×10^{-17}
Input mode cleaner (IMC) optics	2	3	Steel wire	3×10^{-15}
Output mode cleaner (OMC) assembly	2	2	Steel wire	1×10^{-13}
ETM transmission monitor	2	2	Steel wire	2×10^{-12}

Table 2: Suspension parameters for the core optics.

and always tries to keep the differential arm length at zero. Therefore, the “free” displacement, ΔL_{free} will be reduced to a residual length change defined by the response of the detector,

$$\Delta L_{\text{res}} = \frac{\Delta L_{\text{free}}}{1 + G(f)}.$$

The detector response function, $G(f)$, is further broken down into three components: the sensing function $C(f)$, the digital filter function $D(f)$, and the actuation function $A(f)$. Together, these give the open loop transfer function

$$G(f) = A(f)D(f)C(f).$$

318 Fig. 15 shows a block diagram describing the control and calibration system. For a detailed description of how
 319 these functions are modeled and calibrated see [21]. Suffice to say here that once $G(f)$ is known, ΔL_{res} can be
 320 used to find ΔL_{free} , which in turn can be used to calculate the gravitational strain h .

321 One of the key performance metrics of a gravity wave interferometer is the detector noise in the frequency
 322 band of interest. For LIGO, this band is approximately 20Hz to 1000Hz, with peak design sensitivity around
 323 100 Hz. Fig. 16

324 Once $h(t)$ is known, it is possible to begin to search for signatures of gravity waves for a variety of sources,
 325 but the most likely to be seen is from inspirals and mergers of binary systems composed of neutron stars or
 326 black holes. The two events that have been so far identified by LIGO are both binary black hole mergers. The
 327 signature of these events is illustrated in Fig. 17. Note the three distinct stages of the signature. The earliest is
 328 when the black holes are still well separated compared to their Schwartzchild radii, but their mutual orbits
 329 emit gravity radiation. The frequency and amplitude of the radiation gradually ramp up as the black holes

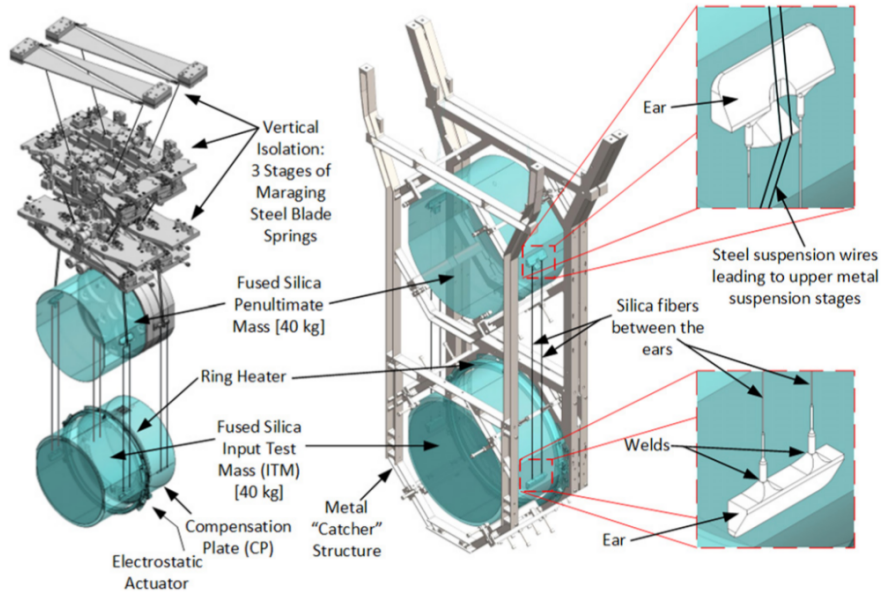


Figure 14: Illustration of the suspension system for the ITM showing the three vertical isolation stages and four pendulum stages. The center image shows the so-called “earthquake-stop”, also known as the catcher structure.

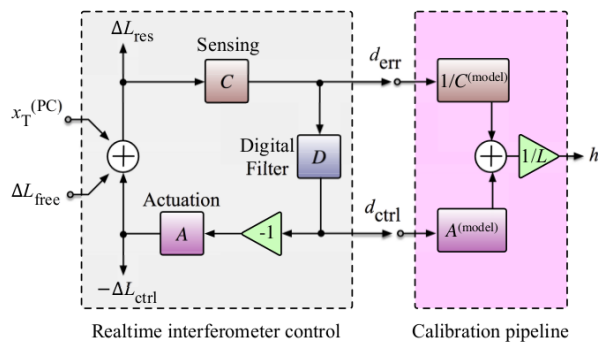


Figure 15: The sensing and control feedback loop of LIGO.

$x_T^{(PC)}$ is a calibration displacement caused by an auxiliary laser source exerting pressure on the test masses.

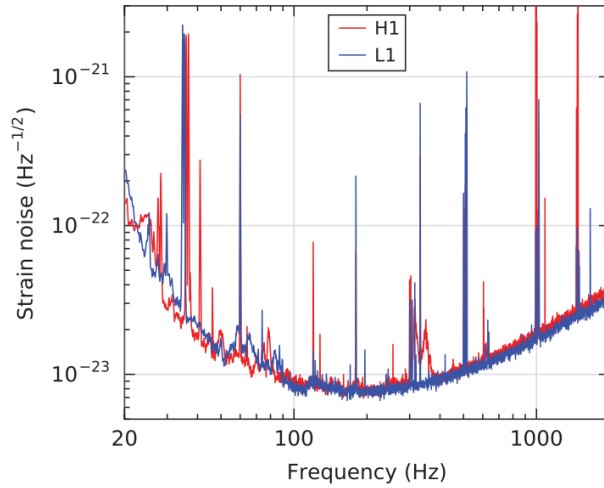


Figure 16: The noise spectral densities for the Hanford (H1) and Livingston (L1) detectors from around the time of the detection of GW150914

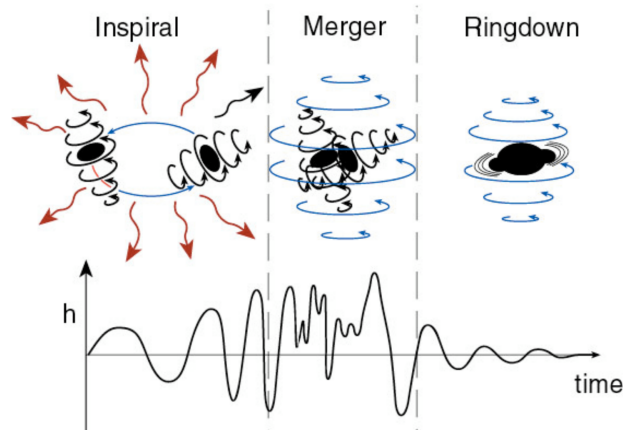


Figure 17: The three stages of binary black hole coalescence

330 orbits become tighter and tighter. Eventually, the black holes get close enough that they merge. This is a
 331 violent, highly non-linear process that requires precise numerical simulations to accurately predict. Finally,
 332 there is the “ringdown” phase where the final black hole radiates away all of its leftover inhomogeneities, or
 333 “hairs”, to reach its stable state where it is defined only by its mass and spin. Approximately 250 thousand
 334 signal waveforms were generated from different mass and spin combinations to be used in matching

335 i. Noise Sources

336

V. OBSERVATIONS

337 i. GW150914

338 ii. GW151226

339

VI. COSMOLOGICAL IMPLICATIONS

340

VII. CONCLUSIONS

341

REFERENCES

- 342 [1] The LIGO Scientific Collaboration. Observation of gravitational waves from a binary black hole merger. *Phys. Rev. Lett.*, 116:061102,
343 Feb 2016.
- 344 [2] The LIGO Scientific Collaboration. Gw151226: Observation of gravitational waves from a 22-solar-mass binary black hole coalescence.
345 *Phys. Rev. Lett.*, 116:241103, Jun 2016.
- 346 [3] Henri Poincare. Sur la dynamique de l'électron. *Proc. Acad. Sci.*, 140:1504–1508, 1905. In French.
- 347 [4] Albert Einstein. Integration neherunswise feldgleichungen der der gravitation. *Sitzungsber. Preuss. Akad. Wiss. Berlin (Math.Phys.)*,
348 22:688–698, 1916. In German.
- 349 [5] Felix A. E. Pirani. Republication of: On the physical significance of the riemann tensor. *General Relativity and Gravitation*, 41(5):1215–
350 1232, 2009.
- 351 [6] Kip Thorne. Caltech physics 237 course notes. online. <http://elmer.tapir.caltech.edu/ph237/>.
- 352 [7] Jorge L. Cervantes-Cota, Salvador Galindo-Uribarri, and George F. Smoot. A brief history of gravitational waves. *Universe*, 2(3), 2016.
- 353 [8] Joseph Weber. The detection and generation of gravity waves. *Physical Review*, 117:306–313, 1960.
- 354 [9] Joseph Weber. Observation of the thermal fluctuations of a gravitational-wave detector. *Physical Review Letters*, 17:1228–1230, 1966.
- 355 [10] Joseph Weber. How i discovered gravitational waves. *Popular Science*, pages 106–107,190–192, May 1972.
- 356 [11] J. H. Taylor, L. A. Fowler, and P. M. McCulloch. Measurements of general relativistic effects in the binary pulsar psr1913 + 16. *Nature*,
357 February 1979.
- 358 [12] R.L. Forward. Wide band laser-interferometer gravitational-radiation experiment. *Phys. Rev. D*, 17:379–390, 1978.
- 359 [13] L. Janna. *Black Hole Blues and Other Songs from Outer Space*. Knopf, New York, NY, USA, 2016.
- 360 [14] R. Russel. Catching the wave. *Sci. Am.*, 266:90–99, 1992.
- 361 [15] C. Davide. Hunt for gravitational waves to resume after massive upgrade: Ligo experiment now has chance of detecting ripples in
362 space-time. *Nature*, 525:301–302, 2015.
- 363 [16] Gires F. and Tournois P. Interferometre utilisable pour la compression d'impulsions lumineuses modulees en frequence. *C. R. Acad.*
364 *Sci. Paris*, 258:6112–6115, Feb 1964.
- 365 [17] The LIGO Scientific Collaboration. Advanced ligo. *Classical and Quantum Gravity*, 32(7):074001, 2015.
- 366 [18] R. W. P. Drever, J. L. Hall, F. V. Kowalski, J. Hough, and G. M. Ford. Laser phase and frequency stabilization using an optical
367 resonator. *Appl. Phys. B*, 31:97–105, 1983.
- 368 [19] Eric D. Black. An introduction to pound-drever-hall laser frequency stabilization. *Am. J. Phys.*, 69:97–105, January 2001.
- 369 [20] Brian J. Meers. Recycling in laser-interferometric gravitational-wave detectors. *Phys. Rev. D*, 38(8):2317–2326, October 1988.
- 370 [21] LIGO Scientific Collaboration. Calibration of the advanced ligo detectors for the discovery of the binary black-hole merger gw150914.
371 *Phys. Rev. D*, 95:062003, Mar 2017.